Earth and Planetary Science Letters 297 (2010) 577–586

Contents lists available at ScienceDirect

Earth and Planetary Science Letters

journal homepage: www.elsevier.com/locate/epsl

Bedrock fracturing, threshold hillslopes, and limits to the magnitude of bedrock landslides

Brian A. Clarke *, Douglas W. Burbank

Department of Earth Science, University of California, Santa Barbara, CA 93106, United States

ARTICLE INFO

Article history:
Received 27 July 2009
Received in revised form 18 June 2010
Accepted 6 July 2010
Available online 31 July 2010

Editor: T.M. Harrison

Keywords:
bedrock fractures
threshold slopes
landslides
landscape evolution
erosion

ABSTRACT

Bedrock fracturing and rock strength are widely believed to influence landscape morphology and erosional resistance. Yet, understanding of the quantitative relationship between rock-mass strength and landscape evolution remains limited. Here we present a new application of seismic refraction surveys that uses variations in seismic velocity to interpret differences in bedrock fracture density with depth. We use a comparative study of Fiordland and the western Southern Alps of New Zealand to examine how differences in rock type and bedrock fracturing influence landscape morphology and landslide response to rock uplift. In both regions, slopes appear invariant with differential rock-uplift rates and slope distributions reveal modal hillslope angles of ~32°. The majority of landslides initiate on slopes steeper than the modal hillslope angle, however, landslide magnitude–frequency distributions reveal order-of-magnitude differences between the regions, with Fiordland experiencing considerably smaller and less frequent landsliding events. Landslide-driven denudation rates of ~9 mm/yr in the western Southern Alps and between ~0.1 and 0.3 mm/yr in Fiordland approximate estimates of long-term rock-uplift rates for each region. The invariance of hillslope angles, near-normal slope distributions, predominance of landslide initiation on slopes steeper than modal values, and the apparent balance between rates of uplift and landslide-driven erosion suggest that hillslopes in both regions are at threshold angles. Their similar modal slopes further suggest that both ranges are characterized by equivalent rock-mass strength, despite striking differences in lithology. Additionally, our seismic analysis reveals nearly identical surface p-wave velocities. The unexpected equivalence of both modal slopes and surface velocities between these lithologically distinct ranges is attributed to contrasting degrees of surface fracturing that have differentially affected the intact rock properties, such that they now yield equivalent surface velocities and hillslope-scale strengths. Given that surface fractures help regulate threshold angles by modulating hillslope strength; we propose that shallow seismic velocities may provide a quantitative proxy for rock-mass strength. We define two contrasting fracture and landsliding environments. In Fiordland, dense geomorphic fracturing that is focused within the shallow subsurface appears to limit the depth and magnitude of most bedrock landslides. Conversely, in the western Southern Alps, tectonic forces produce pervasive fracturing with depth that results in larger, and deeper landslides. Our data suggest that bedrock fracturing at the Earth's surface modulates threshold hillslope angles, whereas the depth of bedrock fracturing influences the magnitude and frequency of landslide response to tectonic rock uplift.

1. Introduction

In tectonically active mountain ranges, in which rates of erosion outpace rates of soil-production, landscapes respond to rock uplift through bedrock landsliding on hillslopes poised at the threshold of stability (Schmidt and Montgomery, 1995; Burbank et al., 1996; Montgomery, 2001). In such landscapes, base-level changes typically drive fluvial and glacial incision of valley bottoms and cause steepening of adjacent hillslopes. This steepening destabilizes hillslopes and induces bedrock landsliding, which limits hillslope gradients to threshold angles of stability (Selby, 1980, 1992; Schmidt and Montgomery, 1995). Sustained rock uplift and valley incision perpetuate this process and result in landslide-dominated hillslope denudation that keeps pace with rates of rock uplift and valley incision while maintaining hillslopes at threshold angles (Burbank et al., 1996; Montgomery and Brandon, 2002).

Threshold landscapes display slopes that are distributed approximately normally about a modal slope value that is dependent on the mechanical strength of hillslope-scale rock masses and is independent of variation in rock uplift or denudation rates that exceed soil-production rates (Burbank et al., 1996; Montgomery, 2001; Korup,

* Corresponding author. Present address: Institute for Earth and Environmental Sciences, Universität Potsdam, Germany 14476. Tel.: +49 331 977 5811; fax: +49 331 977 5700.
E-mail address: clarke@geo.uni-potsdam.de (B.A. Clarke).

0012-821X/$ – see front matter © 2010 Elsevier B.V. All rights reserved.
doi:10.1016/j.epsl.2010.07.011

2008). Rock-mass strength, a metric of mechanical rock strength over a given scale, incorporates the intact (unfractured) rock strength, degree of weathering, and the intensity and characteristics of bedrock fractures (Deere, 1964; Selby, 1980, 1992; Schmidt and Montgomery, 1995; Hoek and Brown, 1997). Rock-mass strength is highly influenced by the weakest unit within the rock mass and by the density, orientation, and spatial distribution of bedrock fractures or discontinuities (Barton et al., 1974; Selby, 1992; Hoek and Brown, 1997). These factors cause rock-mass strength to decrease over increasing spatial scales. Consequently, rock-mass strength at landscape scales has little relation to laboratory measurements of intact rock (Selby, 1992; Schmidt and Montgomery, 1995).

The role of rock strength and the influence of bedrock fractures at hillslope scales are notoriously hard to quantify. Most current methods rely on semi-quantitative classification schemes that assign a range of values to qualitative assessments of outcrop characteristics (e.g., the rock-mass-strength (RMS) classification (Selby, 1980, 1992), Geologic Strength Index (GSI) (Hoek and Brown, 1997), Rock Quality Designation (RQD) (Deere, 1964), and many others). Discussion of rock-mass strength in geologic literature often implicitly refers to one of these classification schemes. Here, however, we refer to rock-mass strength as the actual mechanical strength of a rock mass and not to one of the proxy classification methods.

The influence of rock-mass strength on erosional resistance and landscape evolution is often overlooked or simply incorporated into scaling coefficients in transport equations (Hack, 1957; Carson and Kirkby, 1972). Quasi-quantitative classification schemes, although useful in geoengineering applications, are difficult to incorporate into landscape evolution models or quantitative analysis of the integrated role of tectonic, climatic, and lithologic influences on spatial and temporal patterns of erosion. Although rock-mass strength is typically difficult to quantify, such strength is believed to exert a fundamental control on bedrock erodibility, thresholds of hillslope stability, and patterns of bedrock landsliding (Selby, 1992; Stock and Montgomery, 1999; Duvall et al., 2004; Molnar et al., 2007; Korup and Schlunegger, 2009). Yet, despite this acknowledged importance, we still have a very limited understanding of the mechanistic links between the factors influencing rock-mass strength and the efficiency of erosive processes.

Here we present a comparative analysis of the western Southern Alps and Fiordland regions of New Zealand (Fig. 1), where similar climatic forcing but starkly different rock-uplift rates and underlying lithologies characterize these two side-by-side mountain ranges. Previous comparative studies between these ranges identified the geomorphic imprint of large landslides and contrasts in valley cross-sectional profiles, attributed to rock strength (Augustinus, 1995; Korup, 2005a). We build upon these studies to explore how bedrock mechanical properties influence landscape morphology and erosional response to changes in base level. To assess the broad influence of lithologic and tectonic contrasts between the ranges, we examine variations in topographic characteristics and assess patterns and distributions of landslides and landslide-driven erosion. We then present a new application of shallow seismic refraction surveys that utilizes the magnitude and pattern of p-wave velocity profiles to interpret variations in bedrock fracture densities in the shallow subsurface. We hypothesize that bedrock fracturing in the shallow subsurface strongly influences landscape morphology and landslide response to rock uplift. Through this comparison, we try to improve understanding of the relationship between bedrock fracturing, threshold hillslopes, and the magnitude–frequency distributions of landslides.

2. Study area

The Southern Alps and Fiordland, both located on the west coast of the South Island of New Zealand (Fig. 1), are formed by the oblique convergence of the Pacific and Australian plates (Demets et al., 1990). The Southern Alps comprise detached material derived from the upper portion of the westward-subducting Pacific plate, which is accreted onto the orogenic wedge of the Southern Alps, and thrust up to the surface along the steep, east-dipping Alpine fault (Koons, 1990; Beaumont et al., 1996). The Southern Alps comprise low-grade metamorphic rocks (Fig. 1B) ranging from greywacke in the east to its low-grade schist derivatives in the west (Mason, 1962). In Fiordland, although rock mass is driven upward by the eastward subduction of the Australian plate, rock is not advected through the orogen as occurs in the Southern Alps (Sutherland et al., 2000; Malservisi et al., 2003). Fiordland comprises igneous and high-grade metamorphic rocks with a cap of metasedimentary rock in the range's core (Bradshaw, 1990: Fig. 1B). Fiordland and the Southern Alps experience similar precipitation patterns (Figs. 1 and 2) and have undergone temporally and spatially similar glacial–interglacial transitions throughout the Quaternary (Griffiths and McSaveney, 1983; Suggate, 1990). Whereas the western flanks of both regions receive strikingly high annual precipitation (>8 m/yr in some areas), an orographic gradient sharply reduces precipitation from west to east across both ranges.

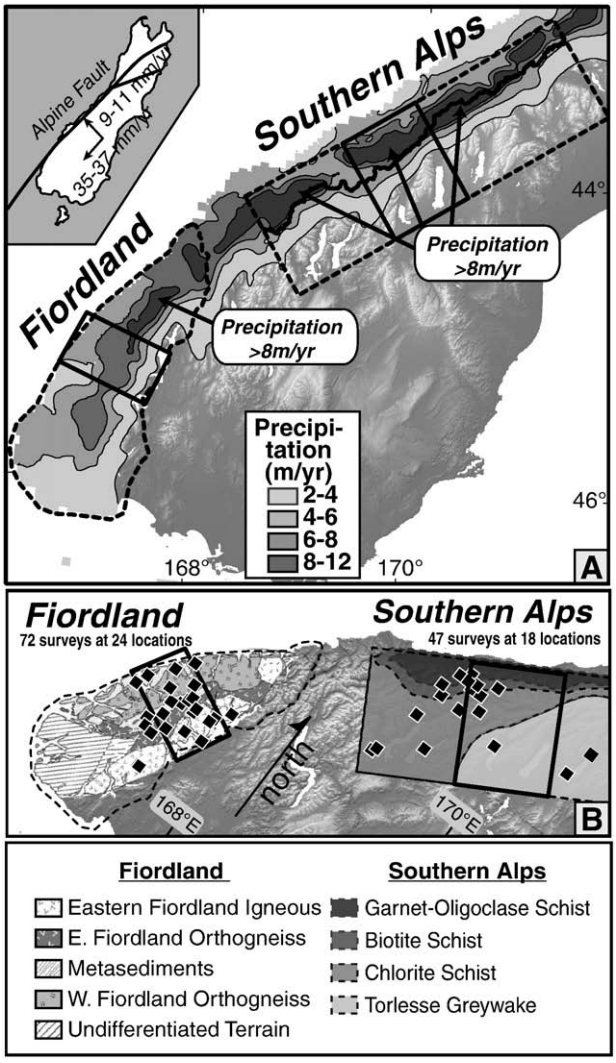

Fig. 1. Location, precipitation, and geology of the Southern Alps and Fiordland regions of New Zealand. A) Patterns of precipitation (NIWA, 2000) and the locations of the two study regions (dashed-lines). Black boxes outline the 40×60 km and 60×80 km swaths through Fiordland and the Southern Alps, respectively. The thick black line shows the location of the Southern Alps drainage divide. Inset shows plate motion relative to the Alpine Fault. B) Locations of seismic survey sites and simplified geologic maps for Fiordland and the Southern Alps. Modified from Bradshaw (1990) and Beaumont et al. (1996).

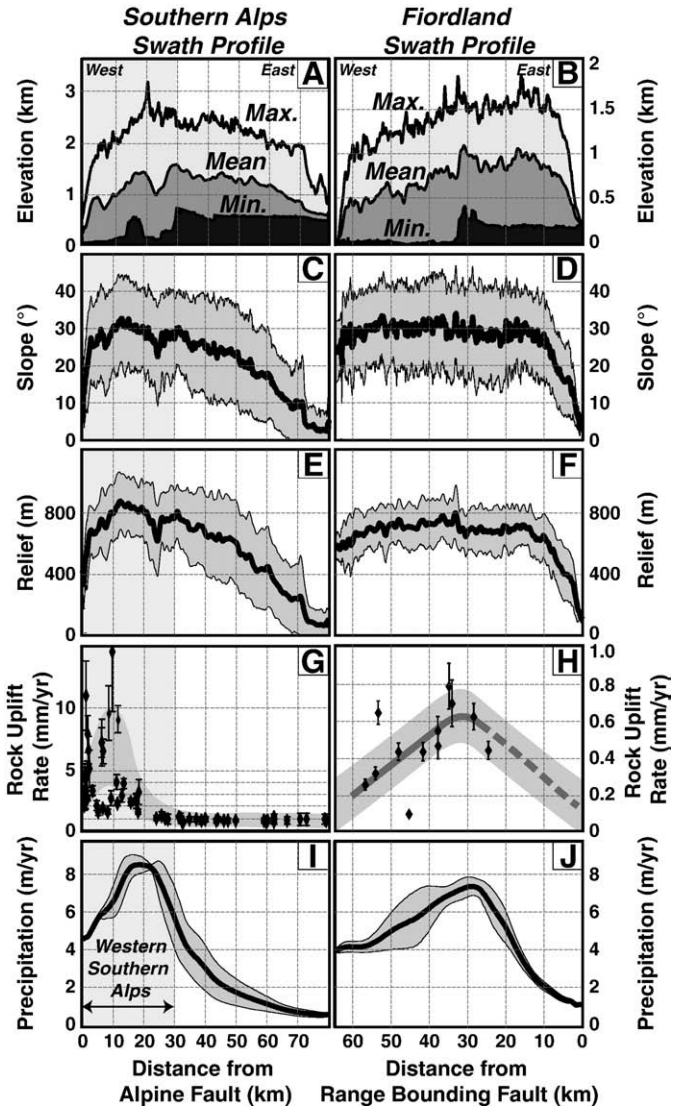

Fig. 2. Swath profiles across the Southern Alps and Fiordland. Swath profiles perpendicular to the range crests (Fig. 1) show maximum, mean and minimum topography (A and B). The mean (thick black line) and standard deviation ($\pm 1\sigma$ shaded) are shown for slope (C and D) from a regional slope grid calculated over 150 m × 150 m areas, and relief (E and F) derived from a 2-km radius analysis window. G and H: Patterns of long-term rock uplift derived from low-temperature cooling ages (Tippett and Kamp, 1993, 1995; House et al., 2002, 2005), the dashed line is the inferred continuation of the trend. I and J: Mean rates of annual precipitation (thick black line) $\pm 1\sigma$ (shaded region) (NIWA, 2000). The western Southern Alps, defined as the area west of the drainage divide and east of the Alpine Fault, occupies the western 30 km of the Southern Alps profiles.

Fiordland and the Southern Alps experience strikingly different long-term rates of exhumation. In the Southern Alps, rates attain 7–11 mm/yr on the rain-soaked west coast and decrease sharply across the divide to the east (Tippett and Kamp, 1993, 1995). Although less well constrained, exhumation rates in Fiordland range between ~0.2 and ~1 mm/yr (House et al., 2002, 2005): ~5 to 20 times slower than those of the Southern Alps.

3. Methods and results

3.1. Geospatial analysis and slope distributions

We assess topographic characteristics of both ranges by examining swath profiles that run perpendicular to the range crests and slope distributions from the entirety of the western Southern Alps and Fiordland study regions (Figs. 1–3). Swath profiles were created for elevation, slope, topographic relief, rock-uplift rates (estimated from thermochronology), and mean annual precipitation (Fig. 2). All topographic data are generated from a 50-m DEM, whereas mean annual precipitation profiles are derived from a dataset with 500-m grid spacing (NIWA, 2000). Swath locations were chosen to encompass the seismic survey sites and to provide representative profiles of the ranges in their entirety. A wider swath width is used in the Southern Alps to account for the strong topographic signal of longitudinal valleys running obliquely to the drainage divide, whereas a narrower swath width is used in Fiordland due to the curvature of the range axis.

The topographic profiles reveal that both ranges have asymmetric geometry with the topographic divide shifted in the direction of subducting plate motion (Fig. 2A, B). In the Southern Alps, this asymmetry has been attributed to tectonic advection of rock mass which drives the topographic divide to the west despite much higher western precipitation (Koons, 1989; Beaumont et al., 1996; Willett, 1999). In Fiordland, the topographic divide is shifted to the east, away from the dominant wind direction.

Slope and topographic relief profiles reveal near uniform mean values across the width of Fiordland (~30° and ~800 m, respectively; Fig. 2D, F). This uniformity is particularly striking given the differences in lithology and rock uplift across the range. In the Southern Alps, mean slopes and relief remain constant between the Alpine Fault in the west and the drainage divide ~30 km to the east (Fig. 2C, E). Similar to Fiordland, mean slopes in this region are maintained at ~30°. East of the Southern Alps drainage divide, both slope and relief steadily diminish. Given such contrasts between the eastern and western Southern Alps, we focus our analysis on the more spatially uniform western Southern Alps. The persistently high mean slope and relief values across both Fiordland and the western Southern Alps may be indicative of threshold slopes that are independent of rock-uplift rates. Conversely, the diminishing mean slope and relief values in the eastern Southern Alps, which comprise similar parent material, are more consistent with predictions for sub-threshold landscapes, where slope angles correlate with rates of uplift and erosion (Strahler, 1950; Burbank, 2002; Montgomery and Brandon, 2002; Binnie et al., 2007; Ouimet et al., 2009).

Profiles of rock-uplift rates across both ranges were deduced from low-temperature thermochronometers. In the Southern Alps (Tippett and Kamp, 1993, 1995), apatite and zircon fission-track ages suggest rates that reach ~7–11 mm/yr west of the drainage divide, but abruptly decrease to the east (Fig. 2G). Both the highest rock uplift rates, associated with the exhumation of higher-grade metamorphic

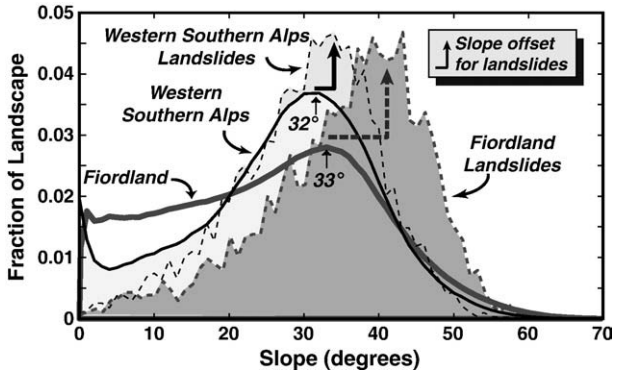

Fig. 3. Slope distributions for the western Southern Alps (thin black line) and Fiordland (thick gray line) reveal similar modal slope values of 32° and 33°, respectively, and near-normal distributions for slopes >20°. Distributions of slopes affected by landslides (dashed lines with shaded interiors) intersect the topographic slope distributions near the modal value and have distribution peaks that are offset towards steeper slopes. These distributions reveal the increased probability of hillslope failure on slopes steeper than the modal slope value of the entire landscape.

rocks, and the highest precipitation rates are focused on the western side of the Southern Alps within ~30 km of the range-bounding Alpine Fault (Koons, 1990; Beaumont et al., 1996). In Fiordland, rock-uplift rates were derived from apatite (U–Th)/He ages (House et al., 2002, 2005) and based on an assumed 70 °C closure temperature, 30 °C/km geothermal gradient, 5 °C temperature at sea-level, and 6 °C/km adiabatic lapse rate. We assume the 70 °C isotherm closely mimics the broad wavelength of the mean topography. We calculate the estimated rock-uplift rate as the vertical distance between the sampling location and the assumed depth to the 70° isotherm divided by the sample age (Fig. 2H). Estimated rock-uplift rates in Fiordland range between ~0.2 and 0.8 mm/yr, with peak rates near the center of the range.

In the Southern Alps, the peak rainfall of >8 m/yr occurs ~10 km west of the drainage divide, whereas in Fiordland, the peak lies 2–5 km to the east of the divide (Fig. 2I, J). Farther east, annual rainfall drops 6 to 8 fold. The steep topographic rise of the western Southern Alps results in a sharp peak in precipitation, whereas in Fiordland, the gradual, west–east topographic rise results in a more dispersed precipitation pattern.

Slope distributions have been widely used to assess landscape characteristics (e.g., Burbank et al., 1996; Montgomery, 2001; Korup, 2008). Montgomery (2001) showed that threshold landscapes display near-normal slope distributions with modal values associated with the mechanical strength of hillslopes. Sub-threshold portions of the landscape, where rates of erosion are less than rates of soil production, display exponentially declining slope distributions. For the entire study region of Fiordland and the western Southern Alps (Fig. 3), slopes were binned in 1° increments and normalized by area. Both regions show strikingly similar modal slope values: 32° in the western Southern Alps and 33° in Fiordland. Although slopes >20° appear near-normally distributed about a regional mode, gentler hillslopes are more common than predicted for threshold landscapes. This pattern may result from analysis of both threshold and sub-threshold regions, an unavoidable inclusion when analyzing entire ranges. This effect is more pronounced for the Fiordland region (Fig. 3), which is not surprising given the greater abundance of low-gradient glacially sculpted valley bottoms in comparison to the more fluvially incised valleys in the western Southern Alps.

Although both regions display slope profiles that appear invariant with differential uplift rates as well as near-normal slope distributions with high modal slope values, as predicted for threshold landscapes, slope characteristics alone are not sufficient to prove threshold states. Further evidence on the style and rates of landsliding is necessary to prove the existence of threshold topography.

3.2. Styles, rates, and magnitudes of bedrock landsliding

In rapidly eroding, unglaciated landscapes, bedrock landslides account for the majority of hillslope erosion in excess of soil-production rates. Rock uplift and valley incision steepen hillslope gradients, thereby destabilizing hillslope material and causing bedrock landslides on slopes steeper than the threshold stability angle. Therefore, threshold slopes should dominate such landscapes, and rates of landslide-driven erosion should approximately balance the rate of rock uplift and valley incision at steady state.

In order to assess the role and rate of bedrock landsliding within the study regions, we examine slope distributions from landslide-affected terrain, assess landslide magnitude–frequency distributions, and compare estimated rates of landslide-driven denudation to long-term rock-uplift. Here, we present a new landslide inventory for Fiordland that we then compare to comparable data from the western Southern Alps (Hovius et al., 1997).

To create a spatially and temporally constrained landslide inventory for Fiordland, we mapped landslide perimeters in ArcGIS for two sets of spatially overlapping, orthorectified air photos from 1965/66 and 2007 (NZ Aerial Mapping Ltd.). The 1965/66 and 2007 photosets have pixel resolutions of 2.0 m and 0.6 m, respectively. Landslides were identified using morphometric criteria and higher surface reflectivity relative to surrounding vegetation. Above tree line (~1000 m), landslide identification becomes difficult due to the lack of vegetation and more homogenous reflectivity. Mapping was, therefore, constrained to elevations <1000 m, yielding an effective map area of 1085 km^2. We identified 2211 landsides that occurred in the 42-yr interval preceding 2007 (Fig. 4). Both the full extent of the landslide scar and the width of the source area were measured. Although width can be estimated as the square root of landslide area (Hovius et al., 1997, 2000; Lavé and Burbank, 2004), we prefer to measure width directly, rather than try to discriminate on an air photo between the source area and the entire the landslide scar.

Several caveats, however, must be addressed in regards to the Fiordland landslide inventory. The data were collected over the entire width of the orogen, and thus provide a spatially and temporally averaged assessment of landsliding over the 42-yr period. This range-scale averaging does not assess the influence of differential erosion or uplift across the width of the range. Revegetation during the 42-yr analysis period may have resulted in undersampling of some small landslides (Stark and Hovius, 2001). Although our analysis focuses on larger landslides, which are less likely to be rendered unmappable due to revegetation over this time period, the influence of small landslides may be underrepresented. Additionally, the 2007 air photos include landslides triggered by the August 22, 2003 M7.2 earthquake that occurred just offshore of the study site (Hancox et al., 2003; McGinty and Robinson, 2007). Seismic shaking may have caused anomalously high rates of landsliding that are not representative of the long-term average. Earthquake-triggered landslides, however, are interpreted to leave a distinct signature on the Fiordland landscape and may be responsible for a significant portion of hillslope erosion in the region (Korup, 2005a,b; Hancox and Perrin, 2009). Given these caveats, the uncertainties in the following landslide analysis are certainly greater than the analytical uncertainty attributed solely to the applied techniques. While acknowledging the inherent uncertainties in these data, we assume that this extensive landslide inventory still provides an accurate first-order assessment of landslide occurrences within the region.

In threshold landscapes, hillslope angles are limited by the strength of the rock mass (Schmidt and Montgomery, 1995), and landslides are expected to preferentially occur on slopes steeper than the modal threshold gradient (Lin et al., 2008). Hillslope angles were

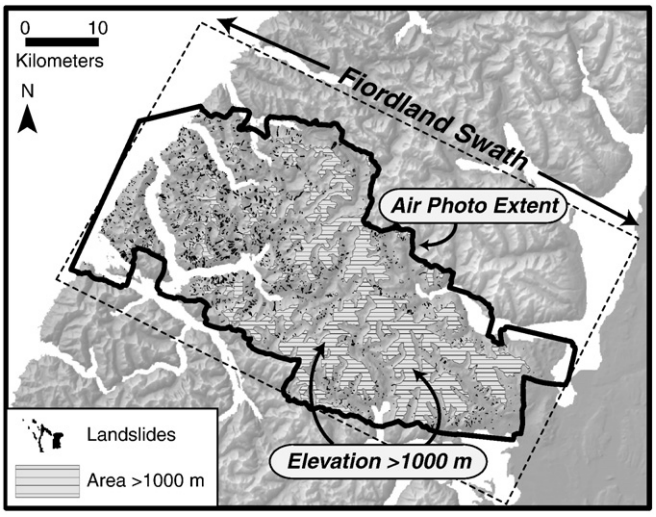

Fig. 4. Location of Fiordland landslides (black-filled polygons) that occurred below 1000 m over the 42-yr analysis interval. Extent of the air photo coverage, regions with elevations >1000 m, and the extent of the Fiordland swath (Fig. 2) are identified.

extracted for each of the mapped landslides, and their distributions (normalized by the number of landslides within each region) were plotted against the slope distributions from the entirety of the study regions (Fig 3). In both ranges, the two distributions intersect roughly at the modal topographic slope value, with landslides predominantly occurring on slopes steeper than these modal values, as predicted for threshold landscapes. This pattern of landslide-affected slopes further suggests that observed modal slope values represent an approximate stability threshold, such that steeper slopes are considerably more likely to fail by landsliding.

In order to assess the efficiency with which landslides modify a landscape, both the size of individual events and the frequency with which different sized events occur need to be examined (Wolman and Miller, 1960; Hovius et al., 1997). Logarithmic landslide magnitude-frequency distributions, normalized by area and time, were calculated (Fig. 5) for both the new Fiordland landslide inventory and the existing landslide data from the western Southern Alps (Hovius et al., 1997). These regional comparisons show order-of-magnitude differences in the largest observed landslide sizes, the rollover length scales (identified by the peak in the distributions), and the overall frequency of large landsliding events (Fig. 5). Although significant differences in the smallest landslides exist between both regions, we focus on landslides larger than the rollover length scales, because larger slides minimize mapping artifacts (Stark and Hovius, 2001; Brardinoni and Church, 2004). Following the methods outlined by Hovius et al. (1997), landslide magnitude–frequency distributions can be described by a power-law function such that,

$$n_c = k(A)^{-\beta}, \tag{1}$$

where n_c is the number of landslides of area A and k is a scaling coefficient that defines the rate of landsliding per area per year (Hovius et al., 1997). The exponent β defines the slope of the power-law trend in log–log space. Power-law regressions were fit to the most robust and linear portions of the log–log distributions, occurring between 10^{-3} and 10^{-1} km^2 in Fiordland and 10^{-2} and 10^{-1} km^2 in the western Southern Alps (Fig. 5). These power-law regressions yield k values of 2.3×10^{-6} km^{-2} yr^{-1} for Fiordland and 5.4×10^{-5} km^{-2} yr^{-1} for the Southern Alps. Ohmori and Hirano (1988) and Hovius et al. (1997) have shown that, when $\beta\leq1.5$, denudation by landsliding is volumetrically dominated by the largest landslide events. The slope exponent, β, for the power-law fits are 1.07 in Fiordland and 1.16 in the western Southern Alps, indicating near-parallel distributions and the importance of large landslides in both regions (Fig. 5).

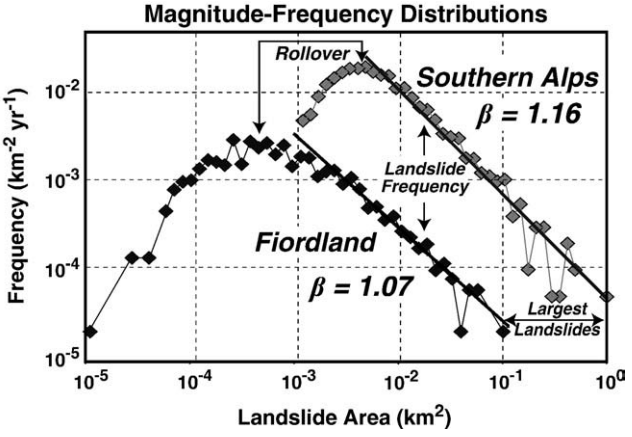

Fig. 5. Landslide magnitude–frequency distributions for the western Southern Alps and Fiordland. The distributions use logarithmic binning of landslide magnitudes. Best-fit power-law trends (with a power-law slope exponent, β) were fit to the linear, large magnitude portions of each distribution. Lines with arrows and labels indicate order-of magnitude differences between the regions.

To calculate volumetric estimates of erosion, a scaling relationship is needed to correlate landslide width and depth. Constraining accurate scaling relationships is the most tenuous step in assessing landslide-derived denudation. Several field studies have produced similar relationships between landslide area, width, and depth, suggesting that these relationships may be broadly applicable to bedrock landslides. Ohmori (1992), Hovius et al. (1997), Lavé and Burbank (2004), and Guzzetti et al (2009) all found a linear relationship between landslide depth, d, and width, w, such that $d=\varepsilon w$; where the scaling coefficient, ε, is 0.05 ± 0.02; suggesting that this coefficient is inherent to landslide process mechanics and is independent of regional influences.

Assuming this coefficient is widely applicable, we can calculate the rate of denudation by landsliding for regions where $\beta\leq1.5$ (Hovius et al., 1997) as,

$$V\approx\frac{2\beta\varepsilon\kappa}{(3-2\beta)}L_1^{3-2\beta}, \tag{2}$$

where V is volume of material removed per area per time, and L_1 is the width of the largest possible landslide. Although the largest landslide occurrence in Fiordland within the 42-yr analysis interval is only ~0.1 km^2, an order-of magnitude smaller than the largest landslides in the Southern Alps, larger remnant landslides of ~1 km^2 that predate the air photos were identified within the study area and have been documented in other studies (Korup, 2005a,b; Hancox and Perrin, 2009). Therefore, in both Fiordland and the western Southern Alps, we initially assume that the largest possible landslide width is equivalent to the width of the largest identified landslides (~1 km). From this analysis, landslide-driven denudation is estimated at 9 ± 4 mm/yr in the western Southern Alps (Hovius et al., 1997) and 0.3 ± 0.1 mm/yr in Fiordland. If instead, for Fiordland, we assume that the largest observed landslide within our 42-yr analysis interval is representative of the largest possible landslides, such that $L_1=(0.1)^{1/2}$, then Eq. (2) yields a more conservative estimate for landslide-driven denudation of 0.1 ± 0.05 mm/yr. Although larger landslides do occur in Fiordland, they may be caused by failure along deep structural discontinuities or uncommon, but unusually large seismic events that are not part of the natural landslide cycle described by the power-law function; thus making this more conservative rate a more appropriate estimate of short-term landslide denudation. Without the longer term records needed to constrain the influence and frequency of very large landslides and considering the additional uncertainties associated with the scaling coefficient and influence of seismically triggered landslides, we interpret that the rate of landslide denudation in Fiordland lies within the range of 0.1 ± 0.05 to 0.3 ± 0.1 mm/yr. These landslide analyses reveal a rough equality between estimated rates of rock uplift and landslide-driven denudation in both regions (Fig. 2G, H) and the prevalence of landslide occurrence on slopes steeper than modal hillslope gradients; which, in combination with the distinctive slope characteristics, provides strong evidence that hillslopes in both Fiordland and the western Southern Alps are at threshold gradients.

3.3. Seismic surveys of bedrock fractures

In order to understand how these two landscapes maintain near-equivalent modal slope angles despite being underlain by strikingly different rock types and experiencing order-of-magnitude differences in the size and frequency of landslides, we need to constrain the factors that modulate rock-mass strength at hillslope scales and explore how they influence threshold landscapes. Because these landscapes comprise contrasting lithologies, we focus on the role of bedrock fracturing in modulating rock-mass strength. We present a new application of shallow seismic refraction surveys that uses p-wave (sound-wave) velocity variations along seismic profiles to interpret gradients in bedrock fracture densities and to provide an integrated hillslope-scale proxy for rock-mass strength. We use (i) field and laboratory

measurements of p-wave velocities[1] in bedrock to assess differences in velocity between broad (10 s of m) and small (cm) length-scales, respectively, and (ii) changes in velocity along seismic profiles from the field to assess depth-dependent patterns of bedrock fracturing at meter scales.[1]

Assessment of rock-mass strength by standard classification methods is notoriously variable, even over individual outcrops, whereas seismic profiles are able to quantitatively integrate all contributing factors. P-wave velocities provide an integrated measure of the intact rock properties and fracture density or pore space of the bedrock and, thus, have been used as a holistic proxy for erodibility (Suzuki, 1982). P-wave velocity is a function of the elastic bulk- and shear-moduli and rock-mass density such that,

$$V_p = \sqrt{\frac{\omega + (4/3)\mu}{\rho}}, \tag{3}$$

where V_p is p-wave velocity, ω is the bulk modulus, μ is the shear modulus, and ρ is density (Mavko et al., 1998; Mussett and Khan, 2000). Although V_p is inversely proportional to $\rho^{1/2}$, increased density results in an even more pronounced increase in the elastic moduli for most rocks, such that denser rocks tend to have faster p-wave velocities (Schön, 1996; Mavko et al., 1998; Mussett and Khan, 2000). Decreases in velocity that correlate with increases in fracture density and porosity support interpretations that fractures and discontinuities systematically reduce elastic properties of rocks causing concomitant decreases in velocity (Schön, 1996; Budetta et al., 2001). Because most rock-strength classifications (e.g., RMS, GSI, RQD) attempt to assess factors that also influence p-wave velocity, such as density, weathering, discontinuities, and fractures, it is not surprising that, in the limited laboratory and drill-core-based experiments where these factors were examined, correlations were found between p-wave velocities and classifications of rock-mass strength (El-Naqa, 1996; Budetta et al., 2001).

We build upon these laboratory-scale results by assessing patterns of p-wave velocities from seismic refraction surveys that span 10–60 m along the surface.[1] These field surveys allow integrative assessment of variations in rock mechanical properties and fracture densities at meter scales that are more relevant to geomorphic processes. Such integration reduces noise and gives greater confidence and significance to measured variability. Most importantly, seismic profiles are not limited to surface exposures, but allow assessment of rock characteristics within the shallow subsurface. We examined p-wave velocities from an array of survey sites that span both the width of each orogen and every major rock unit across them (Fig. 1B). All seismic surveys were collected from linear arrays 10–60 m long. Geophones were placed as directly as possible in contact with bedrock surfaces along flat ridges and valley bottoms in locations where bedrock visibly cropped out along the length of the survey[1] and where regolith, when present, was estimated to always be less than 0.5 m thick. Hand samples were collected from each field site and velocity measurements through 2.5-cm-long cores were made in the laboratory.[1]

For field surveys, when first arrival times of seismic-waves at successive geophone sensors are plotted as a function of distance from the seismic source, the p-wave velocity can be calculated as the reciprocal of the instantaneous slope along the time-distance profile (Fig. 6). Hence, a steep profile gradient in time-distance space indicates a slow velocity, and vice versa. Observed time-distance profiles were matched by a best-fit, second-order polynomial curve.[1] The derivative of this curve was used to assess changes in slope along the profile. We estimate the surface velocity of the field profiles based on the slope of the best-fit curve at the origin. A straight line through successive arrivals in the time–distance plot indicates spatially uniform velocity (Fig. 6A), whereas a line with negative curvature

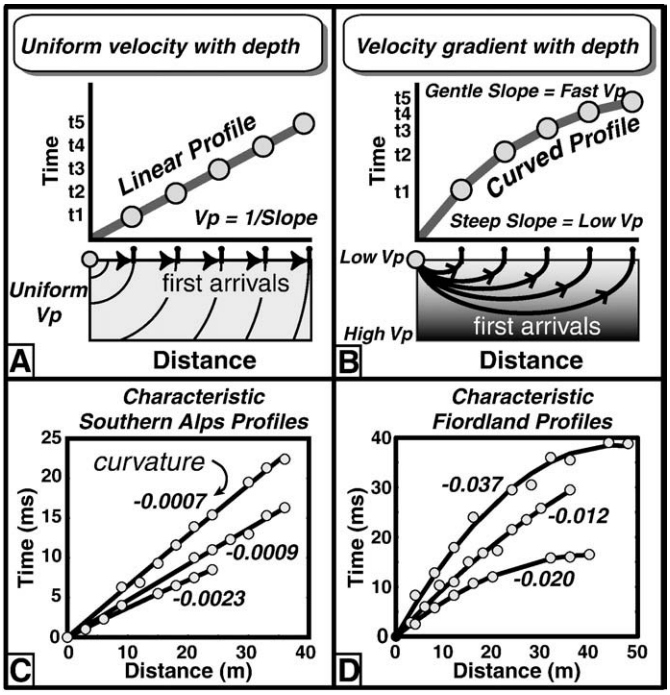

Fig. 6. Schematic seismic survey profiles and time–distance curves. (A) Predicted time–distance data for bedrock with uniform velocity. Lower box represents a vertical shallow subsurface section, where thin black curved lines show seismic wave-front propagation. Black arrows denote the fastest path between the seismic source and each geophone. Upper plot shows the linear time–distance profile due to uniform seismic velocity. *Vp*: p-wave velocity. (B) Schematic seismic survey over bedrock with a velocity gradient (i.e. seismically faster rock with depth). The fastest path from the source to each geophone is curved as the wave path exploits faster velocities at greater depths (curved lines with arrows), resulting in a curved time–distance profile. Examples of time–distance curves for the Southern Alps (C) and Fiordland (D). The black line is the best-fit curve to the measured data (gray dots). Labels indicate the curvature of the best-fit line.

indicates faster velocities with depth that cause refraction of p-waves and curved first-arrival pathways (Fig. 6B). This simple curvature analysis allows us to assess changes in velocity with depth without implementing more complex assumptions and modeling of the shallow subsurface. This analysis does not, however, allow for a simple inversion to determine depth of the wave path. On average, seismic refraction surveys penetrate to depths of about one-third to one-half the length of the survey, equating to estimated depths of ~3–30 m for the surveys presented here.

One premise of the technique is that field measurements provide integrated meso-scale velocity profiles of the shallow subsurface, whereas laboratory measurements provide an estimate of unfractured bedrock velocities for each site. Because field surveys were conducted directly on bedrock surfaces, variations in seismic velocity are interpreted to reveal changes in fracture density with depth.[1] Comparisons between the velocity profiles from field surveys and laboratory measurements of unfractured rock are used to estimate the reduction in field velocities due to bedrock fracturing.

Not surprisingly, average laboratory measurements of p-wave velocities for intact Fiordland samples are almost twice as fast as those for the Southern Alps (Table 1). In contrast, average surface velocities for both regions are strikingly similar at ~1 km/s, despite the different lithologies (Table 1), indicating that, at both sites, bedrock velocities have been reduced to equivalent values. Characteristic arrival-time curves from field surveys in the Southern Alps and Fiordland reveal dramatically different profiles (Fig. 6C, D). In the Southern Alps, nearly linear time-distance profiles are consistent with uniform velocity and fracture densities with depth. In contrast, the Fiordland surveys reveal a high degree of negative curvature, indicating markedly lower

[1] See Supplementary methodological data.

Table 1
Average velocity statistics for the Southern Alps and Fiordland.

	n	Mean lab Vp (km/s)	Mean surface Vp (km/s)	Percent reduction in surface Vp	Mean curvature
Southern Alps	47	2.3 ± 0.09	1.0 ± 0.07	0.57	−0.01 ± 0.001
Fiordland	72	4.0 ± 0.12	0.9 ± 0.06	0.78	−0.03 ± 0.002

All uncertainties are reported as one standard error.

seismic velocities at the surface than at depth. We interpret this contrast to indicate a significant decrease in fracture density with depth in Fiordland versus near-uniform fracturing with depth in the Southern Alps.

This contrast in seismic profile curvature is persistent throughout the survey sites. Frequency distributions of curvature values emphasize the similarities within the individual regions and the differences between them (Fig. 7). In the Southern Alps, 62% of the survey sites have linear profiles, with absolute curvature values <0.01, suggesting that the majority of sites have near-uniform fracture densities with depth. Of the remaining 38% with curvature, they are heavily skewed towards minimum curvature values. In Fiordland, only 1% of the survey sites have a linear profile (absolute curvature <0.01), and 92% have absolute curvature values >0.02 with a larger portion of surveys dispersed over greater absolute curvature values. A Wilcoxon matched-pair test indicates that the two distributions are statistically different ($p<0.1$). These curvature data allow a relative assessment of the depth of pervasive fracturing. In the Southern Alps, the mean profile curvature is −0.01 ± 0.001 (Fig. 7, Table 1), suggesting relatively small changes in velocity due to bedrock fracturing with depth. In Fiordland, the mean profile curvature is three-times greater:

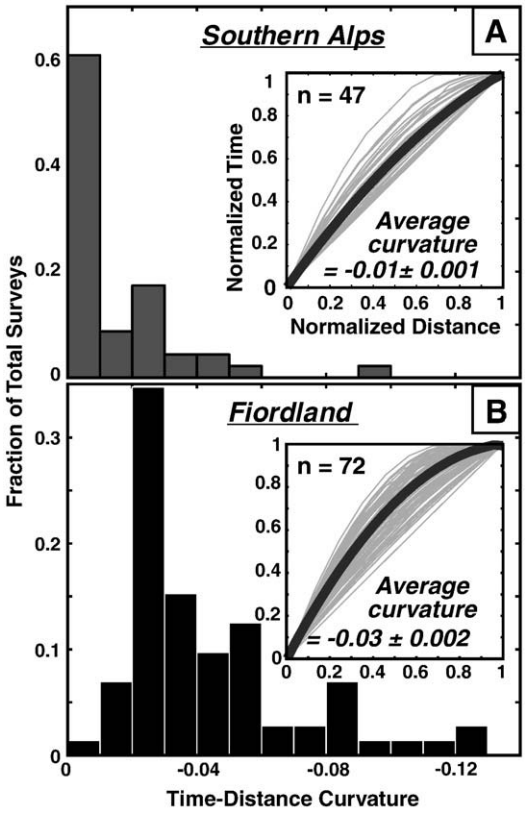

Fig. 7. Seismic time–distance curvature distributions for the Southern Alps (A) and Fiordland (B). Differences in curvature distributions reveal striking contrasts in seismic velocity and interpreted fracture density with depth. Insets show normalized time–distance profiles for all surveys (gray curves) and the normalized average curve (dark line.

−0.03 ± 0.002, indicating much more pronounced velocity gradients and substantial decreases in fracture densities with depth.

We can use differences between the field and laboratory velocities to show that, in both regions, the field velocities in the very shallow subsurface have been significantly reduced relative to the laboratory-based velocity measurements of intact bedrock (Table 1). In the Southern Alps, average surface velocity is ~2.5 times lower than average intact lab velocity. In Fiordland, average surface velocity is reduced five-fold. These dramatic reductions in p-wave velocity indicate that both regions are severely fractured at the surface and that the low velocities are not simply due to weak, low-velocity, intact rock.

In sum, the seismic velocity measurements, curvature distributions (Fig. 7), and mean regional statistics (Table 1) indicate that p-wave velocity in both regions is significantly reduced by highly fractured bedrock in the shallow subsurface. Despite significant surface velocity reductions in both regions, the five-fold reduction of strong, seismically fast, intact rock from Fiordland versus the 2.5-fold reduction in weaker, seismically slower, intact rock from the Southern Alps suggests more intense fracturing of the Fiordland surface, which ultimately results in remarkably similar mean surface velocities of ~1 km/s in both regions. Fracture density in Fiordland, however, appears to rapidly decrease with depth as revealed by curved p-wave velocity profiles that trend toward faster velocities associated with more intact bedrock, whereas in the Southern Alps, high fracture densities and reduced p-wave velocities persist to much greater depths.

These interpretations depend, however, on some poorly quantified uncertainties.[1] Primary among them are changes in subsurface, seismic anisotropy and the influence of ground water or soil/low-velocity cover. Both ground water and soil/cover typically produce time-distance profiles with distinct slope breaks between linear profile sections. Yet, none of our surveys display such characteristics. Similarly, the highly foliated, anisotropic rock of the Southern Alps overwhelmingly displays linear seismic profiles, suggesting that any changes in anisotropy, at the scale of our surveys, have minimal to negligible influence on these profiles. Conversely, Fiordland is dominated by curved profiles despite the more isotropic granites and gneisses that are not expected to produce significant velocity gradients in the absence of fractures and/or weathering. Although such unquantified variables increase the analytical uncertainty of the method, we argue that our data still identify significant trends and enable a reliable first-order assessment of the patterns of bedrock fracturing in the shallow subsurface.[1]

4. Discussion

In order to better constrain the influence of rock properties on landscape development in Fiordland and the western Southern Alps of New Zealand, we compare topographic characteristics, styles and distributions of bedrock landslides, and patterns of bedrock fracturing derived from seismic refraction surveys. The combination of uniform slope profiles that appear invariant with uplift rates, near-normally distributed slopes (>20°) with equivalent modal values of ~32°, the predominance of landslide activity on slopes steeper than modal hillslope angles, and the rough equivalence between rock uplift and landslide-driven denudation rates reveal the signature characteristics of threshold slopes in both regions (Burbank et al., 1996; Montgomery, 2001).

The similarity in modal slope values, however, is surprising given the striking differences in lithologies. Additionally, the landslide magnitude–frequency distributions (Fig. 5) reveal order-of-magnitude differences, with Fiordland experiencing considerably smaller and less frequent landsliding events. We attempt to reconcile this conspicuous similarity in modal slope values and differences in the landslide

distributions by examining the influence of bedrock fracturing on these threshold landscapes.

Because hillslope stability is controlled by the mechanical strength of rocks, the weakest unit within the rock-mass typically governs threshold angles (Selby, 1992; Schmidt and Montgomery, 1995). Therefore, similar to a pile of sand, which cannot be steepened beyond the angle of repose without sloughing off surface material to reduce surface slopes, threshold slopes in regions where the weakest rock is located at the surface or where rock strength is uniform with depth are ultimately governed by surface strength. Even in such regions, however, it is possible to induce deeper landslides through seismic shaking or rainfall-induced increases in hydrostatic pore pressure (Densmore and Hovius, 2000; Iverson, 2000; Meunier et al., 2008). Although fracturing at depth reduces rock strength and increases pore-space, as long as surface strengths are equal to or lower than those at depth, the weaker surface material will still govern the maximum stabile gradient. Therefore, we propose that the density of surface fractures influences threshold angles of stability, whereas the depth of bedrock fracturing limits the magnitude of landslides.

The similar modal slopes within both study regions suggest similar surface rock-mass strength. Seismic surveys of the shallow subsurface reveal that the mean surface velocities of the two regions are also equivalent at ~1 km/s. These similarities suggest that differential surface fracturing between the regions has resulted in equivalent surface bedrock strengths and seismic velocities. Both rock-mass strength and p-wave velocity are influenced by the intact rock strength and density of bedrock fractures. Therefore, strong, but highly fractured bedrock can have a comparable strength and p-wave velocity to weaker, less fractured bedrock. This contention is consistent with the five-fold surface velocity reduction in Fiordland compared to the 2.5-fold reduction in the Southern Alps (Table 1), which result in equivalent mean surface strengths and velocities. We suggest, therefore, that similar to laboratory-scale studies (Schön, 1996; Budetta et al., 2001), large-scale measures of p-wave velocity correlate with rock-mass strength and may provide a quantitative and efficient means to assess the mechanical strength of hillslopes.

The proposed scaling relationships between landslide area, width, and depth (Ohmori and Hirano, 1988; Ohmori, 1992; Hovius et al., 1997; Lavé and Burbank, 2004) imply that differences in landslide magnitude can be interpreted as differences in landslide depth. The magnitude–frequency distributions for Fiordland and the western Southern Alps show ten-fold differences in the largest observed landslides and the overall frequency of landsliding over a 42-yr period (Fig. 5). Based on these distributions and width-depth scaling estimates, Fiordland is clearly dominated by shallower landsliding events in which the largest observed events are limited to estimated depths <15 m. In comparison, the western Southern Alps are characterized by significantly deeper landslides with maximum estimated depths reaching ~50 m. Depth-dependent patterns of fracturing derived from seismic profiles may explain the cause of these striking differences in landslide magnitude. In Fiordland, the average profile curvature of -0.03 ± 0.002 and the fact that 92% of surveys reveal absolute curvatures >0.02 indicate that, although bedrock is highly fractured at the surface, fracture densities decrease sharply with depth. In the Southern Alps, the average profile curvature is only -0.01 ± 0.001 and almost two-thirds of the surveys are characterized by linear trends, indicating both uniform and pervasive fracturing with depth. We interpret these patterns of bedrock fracturing to strongly influence the depth of bedrock landslides. Bedrock failure is most likely to occur where intense fracturing has reduced rock-mass strength. Therefore, bedrock fracturing that is focused near the surface, as in Fiordland, is more likely to cause shallower failures within this fractured zone, rather than deeper failures within more intact bedrock. In contrast, landslide occurrence in bedrock that has been ubiquitously fractured to greater depths, as in the Southern Alps, is not limited by depth-dependent contrasts in rock-mass strength, and, therefore, more readily produces large, deep bedrock landslides. Although in both these threshold landscapes, rates of landslide-driven denudation are governed by rates of rock uplift and valley incision, the particular balance between the magnitude and frequency of bedrock landsliding that achieves these rates (Wolman and Miller, 1960) appears to be strongly influenced by the depth of bedrock fracturing.

Our results suggest that these two landscapes are characterized by two distinctly different modes of bedrock fracturing that may help modulate the size and frequency of landslides, govern the threshold angle of stability, and influence landscape responses to climatic and tectonic forcing. Based on the interpreted patterns of bedrock fracturing, we propose two conceptual models for bedrock-fracture genesis to explain the contrasts between the two regions: 1) tectonic fracturing and 2) geomorphic fracturing (Fig. 8). Tectonic forces can fracture bedrock at depth and then drive the fractured rock to the surface. Molnar et al. (2007) described this process as the "tectonic rock crusher" in which zones of dense fracturing are produced by pushing material along nonplanar faults such that off-fault fracturing is required to accommodate the stresses induced by folding. Conversely, geomorphic processes induce bedrock fracturing from the surface down, thereby enhancing the fracture density within the shallow subsurface. Thermal, biotic, and chemical processes can create new fractures or exacerbate preexisting fractures within a few meters of the surface (Walder and Hallet, 1985; Hales and Roering, 2005, 2007; Delunel et al., 2010). Similarly, internal stresses induced by surface curvature and steep relief can cause near-surface jointing and fracturing (Augustinus, 1995; Miller and Dunne, 1996; Martel, 2006). Whereas the strength of intact rock may determine the rate at which fractures form, tectonic and/or geomorphic fracturing mechanisms reduce that strength and modulate threshold slope angles and landslide magnitudes.

Although this study focuses on landslide-driven erosive processes, the contrasting fracturing mechanisms and resultant patterns in fracture densities observed here should profoundly influence bedrock resistance and erosional efficiency of all surface processes. The simple notion that disintegrated or highly fractured bedrock is more easily eroded than intact bedrock (Gilbert, 1877; Carson and Kirkby, 1972; Molnar et al., 2007; Moore, et al., 2009; Dühnforth et al., 2010) suggests that the shallow seismic techniques used here to interpret

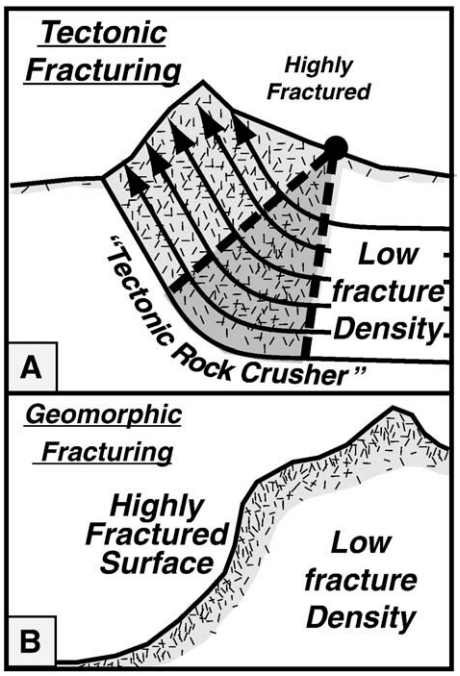

Fig. 8. Conceptual models of two modes of bedrock fracturing. (A) The "tectonic rock crusher" model (modified from Molnar et al., 2007) and (B) surface-down geomorphic fracturing.

bedrock fracture densities may also be applied to other landscapes in order to assess bedrock erodibility (Suzuki, 1982). Future work examining the relationship between patterns of bedrock fractures and rock-mass strength might promote a better understanding of the predominant factors governing hillslope stability, landscape morphology, and the efficiency of erosive processes.

5. Conclusion

We contend that both Fiordland and the western Southern Alps of New Zealand represent threshold landscapes dominated by landslide denudation. Both regions exhibit strikingly similar threshold stability angles of ~32°, despite their significantly different rock types, and display ten-fold differences in the magnitude of the largest landslides. We develop a new application of seismic refraction surveys that uses variations in seismic velocity to interpret differences in bedrock fracture patterns within the shallow subsurface. We infer that differing degrees of bedrock fracturing at the surface of both ranges has reduced both the surface strength and surface p-wave velocity of the different rock types to equivalent values. This equivalence further suggests that p-wave velocities may provide a quantitative proxy for measures of hillslope-scale rock-mass strength. Differences in landslide magnitudes between the regions are attributed to differences in depth-dependent fracture patterns. In the western Southern Alps, large, deep landslides are interpreted to be the result of deep, pervasive, tectonic fracturing of bedrock. In Fiordland, conversely, geomorphic fracturing, confined to the shallow subsurface, is interpreted to limit landslide depths to within this shallow fractured zone.

Overall, the density of surface fractures appears to govern the threshold angle of hillslope stability, whereas differences in fracture density with depth appear to limit the depths of bedrock landslides, effectively controlling hillslope morphology and the size and frequency of landsliding in response to tectonically driven rock uplift in threshold landscapes.

Acknowledgements

We would like to thank Mark Collar for assistance mapping and analyzing the Fiordland landslides in GIS, and Jordan Lewis and Colin Amos for assistance collecting field seismic surveys. We are grateful to Gary Mavko and the Stanford Rock Physics group for guidance and assistance with laboratory velocity measurement. We thank Fiordland Ecology Holidays, Fiordland Helicopters, the University of Canterbury, and the Fiordland DOC office for field and logistical support. Tom Dunne, Bodo Bookhagen, Tim Stern, and Ralph Archuleta provided valuable input and discussion. Niels Hovius, Steven Binnie, and an anonymous reviewer gave insightful comments and reviews that greatly improved this manuscript. This project was funded by the National Geographic Society, NSF (EAR 0117242), and the Petroleum Research Fund (41960-AC8).

Appendix A. Supplementary data

Supplementary data associated with this article can be found, in the online version, at 10.1016/j.epsl.2010.07.011.

References

Augustinus, P.C., 1995. Glacial valley cross-profile development: the influence of in situ rock stress and rock mass strength, with examples from the Southern Alps, New Zealand. Geomorphology 14, 87–97.
Barton, N., Lien, R., Lunde, J., 1974. Engineering classification of rock masses for the design of tunnel support. Rock Mech. Supp. 6, 189–236.
Beaumont, C., Kamp, P.J.J., Hamilton, J., Fullsack, P., 1996. The continental collision zone, South Island, New Zealand: comparison of geodynamical models and observations. J. Geophys. Res. 101, 3333–3359.
Binnie, S.A., Phillips, W.M., Summerfield, M.A., Fifield, L.K., 2007. Tectonic uplift, threshold hillslopes, and denudation rates in a developing mountain range. Geology 35, 743–746.
Bradshaw, J.Y., 1990. Geology of crystalline rocks of Northern Fjordland—details of the granulite facies western Fjordland Orthogneiss and associated rock units. New Zeal J. Geol. Geophys. 33, 465–484.
Brardinoni, F., Church, M., 2004. Representing the landslide magnitude–frequency relation: Capilano River Basin, British Columbia. Earth Surf. Process. Landf. 29, 115–124.
Budetta, P., De Riso, R., De Luca, C., 2001. Correlations between jointing and seismic velocities in highly fractured rock masses. Bull. Eng. Geol. Environ. 60, 185–192.
Burbank, D.W., 2002. Rates of erosion and their implications for exhumation. Mineral. Mag. 66, 25–52.
Burbank, D.W., Leland, J., Fielding, E., Anderson, R.S., Brozovic, N., Reid, M.R., Duncan, C., 1996. Bedrock incision, rock uplift and threshold hillslopes in the northwestern Himalayas. Nature 379, 505–510.
Carson, M.A., Kirkby, M.J., 1972. Hillslope Form and Process. University Press, London, England.
Deere, D.U., 1964. Technical descriptions of rock cores for engineering purposes. Rock Mech. Rock Eng. 1, 107–116.
Delunel, R., van der Beek, P.A., Carcaillet, J., BourlÈs, D.L., Valla, P.G., 2010. Frost-cracking control on catchment denudation rates: insights from in situ produced 10Be concentrations in stream sediments (Ecrins-Pelvoux massif, French Western Alps). Earth Planet. Sci. Lett. 293, 72–83.
Demets, C., Gordon, R.G., Argus, D.F., Stein, S., 1990. Current plate motions. Geophys. J. Int. 101, 425–478.
Densmore, A.L., Hovius, N., 2000. Topographic fingerprints of bedrock landslides. Geology 28, 371–374.
Dühnforth, M., Anderson, R.S., Ward, D., Stock, G.M., 2010. Bedrock fracture control of glacial erosion processes and rates. Geology 38, 423–426.
Duvall, A., Kirby, E., Burbank, D., 2004. Tectonic and lithologic controls on bedrock channel profiles and processes in coastal California. J. Geophys. Res. 109, F03002. doi:10.1029/02003JF000086.
El-Naqa, A., 1996. Assessment of geotechnical characterization of a rock mass using a seismic geophysical technique. Geotech. Geol. Eng. , pp. 291–305.
Gilbert, G.K., 1877. Report on the Geology of the Henry Mountains: Geographical and Geological Survey of the Rocky Mountain Region. U.S. Gov. Print. Office, Washington D.C., pp. 93–144.
Griffiths, G.A., McSaveney, M.J., 1983. Distribution of mean annual precipitation across some steepland regions of New-Zealand. New Zeal. J. Sci. 26, 197–209.
Guzzetti, F., Ardizzone, F., Cardinali, M., Rossi, M., Valigi, D., 2009. Landslide volumes and landslide mobilization rates in Umbria, central Italy. Earth Planet. Sci. Lett. 279, 222–229.
Hack, J.T., 1957. Studies of longitudinal stream profiles in Virginia and Maryland. U. S. Geological Survey Professional Paper, Report: P.
Hales, T.C., Roering, J.J., 2005. Climate-controlled variations in scree production, Southern Alps, New Zealand. Geology 33, 701–704.
Hales, T.C., Roering, J.J., 2007. Climatic controls on frost cracking and implications for the evolution of bedrock landscapes. J. Geophys. Res. 112.
Hancox, G.T., Perrin, N.D., 2009. Green Lake Landslide and other giant and very large postglacial landslides in Fiordland, New Zealand. Quat. Sci. Rev. 28, 1020–1036.
Hancox, G.T., Cox, S.C., Turnbull, I.M., Crozier, M.J., 2003. Reconnaissance studies of landslides and other ground damage caused by the Mw7.2 Fiordland earthquake of 22 August 2003. Institute of Geological and Nuclear Sciences science report 2003/30, p. 32.
Hoek, E., Brown, E.T., 1997. Practical estimates of rock mass strength. Int. J. Rock Mech. Min. Sci. Geomech. Abstr. 34, 1165–1186.
House, M.A., Gurnis, M., Kamp, P.J.J., Sutherland, R., 2002. Uplift in the Fiordland region, New Zealand: implications for incipient subduction. Science 297, 2038–2041.
House, M.A., Gurnis, M., Sutherland, R., Kamp, P.J.J., 2005. Patterns of Late Cenozoic exhumation deduced from apatite and zircon U–He ages from Fiordland, New Zealand. Geochem. Geophys. Geosyst. 6, Q09013. doi:10.1029/2005GC000968.
Hovius, N., Stark, C.P., Allen, P.A., 1997. Sediment flux from a mountain belt derived by landslide mapping. Geology 25, 231–234.
Hovius, N., Stark, C.P., Chu, H.T., L., J.-C., 2000. Supply and removal of sediment in a landslide-dominated mountain belt: Central Range, Taiwan. J. Geol. 108, 73–90.
Iverson, R.M., 2000. Landslide triggering by rain infiltration. Water Resour. Res. 36, 1897–1910.
Koons, P.O., 1989. The topographic evolution of collisional mountain belts: a numerical look at the Southern Alps, New Zealand. Am. J. Sci. 289, 1041–1069.
Koons, P.O., 1990. 2-sided orogen—collision and erosion from the sandbox to the Southern Alps, New-Zealand. Geology 18, 679–682.
Korup, O., 2005a. Geomorphic imprint of landslides on alpine river systems, southwest New Zealand. Earth Surf. Process. Landf. 30, 783–800.
Korup, O., 2005b. Distribution of landslides in southwest New Zealand. Landslides 2, 43–51.
Korup, O., 2008. Rock type leaves topographic signature in landslide-dominated mountain ranges. Geophys. Res. Lett. 35, L11402. doi:10.1029/12008GL034157.
Korup, O., Schlunegger, F., 2009. Rock-type control on erosion-induced uplift, eastern Swiss Alps. Earth Planet. Sci. Lett. 276, 278–285.
Lavé, J., Burbank, D.W., 2004. Denudation processes and rates in the Transverse Ranges, southern California: erosional response of a transitional landscape to external and anthropogenic forcing. J. Geophys. Res. 109. doi:10.1029/2003JF000023.
Lin, G.W., Chen, H., Hovius, N., Horng, M.J., Dadson, S., Meunier, P., Lines, M., 2008. Effects of earthquake and cyclone sequencing on landsliding and fluvial sediment transfer in a mountain catchment. Earth Surf. Process. Landf. 33, 1354–1373.

Malservisi, R., Furlong, K.P., Anderson, H., 2003. Dynamic uplift in a transpressional regime: numerical model of the subduction area of Fiordland, New Zealand. Earth Planet. Sci. Lett. 206, 349–364.
Martel, S.J., 2006. Effect of topographic curvature on near-surface stresses and application to sheeting joints. Geophys. Res. Lett. 33. doi:10.1029/2005gl024710.
Mason, B., 1962. Metamorphism in the Southern Alps of New Zealand. Bull. Am. Mus. Nat. Hist. 123, 217–248.
Mavko, G., Mukerji, T., Dvorkin, J., 1998. The Rock Physics Handbook: Tools for Seismic Analysis in Porous Media. Cambridge University Press, New York.
McGinty, P., Robinson, R., 2007. The 2003 Mw7.2 Fiordland subduction earthquake, New Zealand; aftershock distribution, main shock fault plane and static stress changes on the overlying Alpine Fault. Geophys. J. Int. 169, 579–592.
Meunier, P., Hovius, N., Haines, J.A., 2008. Topographic site effects and the location of earthquake induced landslides. Earth Planet. Sci. Lett. 275, 221–232.
Miller, D.J., Dunne, T., 1996. Topographic perturbations of regional stresses and consequent bedrock fracturing. J. Geophys. Res. 101, 25523–25536.
Molnar, P., Anderson, R.S., Anderson, S.P., 2007. Tectonics, fracturing of rock, and erosion. J. Geophys. Res. 112, F03014. doi:10.1029/02005JF000433.
Montgomery, D.R., 2001. Slope distributions, threshold hillslopes, and steady-state topography. Am. J. Sci. 301, 432–454.
Montgomery, D.R., Brandon, M.T., 2002. Topographic controls on erosion rates in tectonically active mountain ranges. Earth Planet. Sci. Lett. 201, 481–489.
Moore, J.R., Sanders, J.W., Dietrich, W.E., Glaser, S.D., 2009. Influence of rock mass strength on the erosion rate of alpine cliffs. Earth Surf. Process. Landf. 34, 1339–1352.
Mussett, A.E., Khan, M.A., 2000. Looking into the Earth; an introduction to geological geophysics.
NIWA, 2000. Mean annual precipitation data (1971–2000) provided by the National Institute of Water and Atmospheric Research. http://www.niwa.co.nz 2000.
Ohmori, H., 1992. Morphological characerstics of the scar created by large-scale rapid mass movement. Japan. Geomorph. Un. Trans. 13, 185–202.
Ohmori, H., Hirano, M., 1988. Magnitude, frequency and geomorphological significance of rocky mud flow, landcreep and the collapse of steep slopes. Z. Geomorphol. Supp. 67, 55–65.
Ouimet, W.B., Whipple, K.X., Granger, D.E., 2009. Beyond threshold hillslopes: channel adjustment to base-level fall in tectonically active mountain ranges. Geology 37, 579–582.
Schmidt, K.M., Montgomery, D.R., 1995. Limits to relief. Science 270, 617–620.
Schön, J.H., 1996. Physical Properties of Rocks—Fundamenals and Principales of Petrophysics. Pergamon, Oxford, UK.
Selby, M.J., 1980. A rock mass strength classification for geomorphic purposes: with tests from Antarctica and New Zealand. Z. Geomorphol. 24, 31–51.
Selby, M.J., 1992. Hillslope Materials and Processes. University Press, Oxford.
Stark, C.P., Hovius, N., 2001. The characterization of landslide size distributions. Geophys. Res. Lett. 28, 1091–1094.
Stock, J.D., Montgomery, D.R., 1999. Geologic constraints on bedrock river incision using the stream power law. J. Geophys. Res. 104, 4983–4993.
Strahler, A.N., 1950. Equilibrium theory of erosional slopes approached by frequency distribution analysis; Part II. Am. J. Sci. 248, 800–814.
Suggate, R.P., 1990. Late Pliocene and Quaternary Glaciations of New-Zealand. Quat. Sci. Rev. 9, 175–197.
Sutherland, R., Davey, F., Beavan, J., 2000. Plate boundary deformation in South Island, New Zealand, is related to inherited lithospheric structure. Earth Planet. Sci. Lett. 177, 141–151.
Suzuki, T., 1982. Rate of lateral planation by Iwaki River, Japan. Trans. Jpn Geomorphol. Union 3, 1–24.
Tippett, J.M., Kamp, P.J.J., 1993. Fission-track analysis of the Late Cenozoic vertical kinematics of Continental Pacific Crust, South Island, New-Zealand. J. Geophys. Res. 98, 16119–16148.
Tippett, J.M., Kamp, P.J.J., 1995. Geomorphic evolution of the Southern Alps, New-Zealand. Earth Surf. Process. Landf. 20, 177–192.
Walder, J., Hallet, B., 1985. A theoretical-model of the fracture of rock during freezing. Geol. Soc. Am. Bull. 96, 336–346.
Willett, S.D., 1999. Orogeny and orography: the effects of erosion on the structure of mountain belts. J. Geophys. Res. 104, 28957–28981.
Wolman, M.G., Miller, J.P., 1960. Magnitude and frequency of forces in geomorphic processes. J. Geol. 68, 54–74.